Environmental Science & Technology

Caltech Library

Subscriber access provided by Caltech Library

Treatment and Resource Recovery

In-situ-generated reactive oxygen species in pre-charged titania and tungsten trioxide composite catalyst membrane filters: Application to As(III) oxidation in the absence of irradiation

Jiyeon Park, Jonghun Lim, Yiseul Park, Dong Suk Han, Hokyong Shon, Michael R Hoffmann, and Hyunwoong Park

Environ. Sci. Technol., **Just Accepted Manuscript** • DOI: 10.1021/acs.est.0c01550 • Publication Date (Web): 16 Jun 2020

In-situ-generated reactive oxygen species in pre-charged titania and tungsten trioxide composite catalyst membrane filters: Application to As(III) oxidation *in the absence of irradiation*

Ji Yeon Park,[a,ψ] Jonghun Lim,[b,ψ] Yiseul Park,[c] Dong Suk Han,[d] Ho Kyong Shon,[e] Michael R. Hoffmann,[b] and Hyunwoong Park[a,*]

[a] *School of Energy Engineering, Kyungpook National University, Daegu 41566, Korea*

[b] *Linde + Robinson Laboratories, California Institute of Technology, Pasadena, California 91125, United States*

[c] *Department of Chemical Engineering, Pukyong National University, Busan 48513, Korea*

[d] *Center for Advanced Materials, Qatar University, Doha 2713, Qatar*

[e] *Centre for Technology in Water and Wastewater, School of Civil and Environmental Engineering, University of Technology Sydney, Australia*

* To whom correspondence should be addressed (H. Park)

E-mail: hwp@knu.ac.kr; Tel: +82-53-950-8973

ψThese authors contributed equally to this work.

Keywords

Solar charging; Reactive oxygen species; Composites; Membrane filters; Charge storage

Abstract

This study demonstrates that in situ-generated reactive oxygen species (ROSs) in pre-photocharged TiO_2 and WO_3 (TW) composite particle-embedded inorganic membrane filters oxidize arsenite (As(III)) into arsenate (As(V)) without any auxiliary chemical oxidants under ambient conditions in the dark. TW membrane filters have been charged with UV or simulated sunlight and subsequently transferred to a once-through flow-type system. The charged TW filters can transfer the stored electrons to dissolved O_2, producing ROSs that mediate As(III) oxidation in the dark. Dramatic inhibition of As(V) production with O_2 removal or addition of ROS quenchers indicates an ROS-mediated As(III) oxidation mechanism. Electron paramagnetic spectroscopic analysis has confirmed the formation of the $HO_2^{\bullet}/O_2^{\bullet-}$ pair in the dark. The WO_3 fraction in the TW filter significantly influences the performance of the As(III) oxidation, while As(V) production is enhanced with increasing charging time and solution pH. The As(III) oxidation is terminated when the singly charged TW filter is fully discharged; however, recharging of TW recovers the catalytic activity for As(III) oxidation. The proposed oxidation process using charged TW membrane filters is practical and environmentally benign for the continuous treatment of As(III)-contaminated water during periods of unavailability of sunlight.

Introduction

Photocatalytic water treatment has been extensively studied over the last few decades and has proven to be capable of remediating most (in)organic chemicals via redox reactions.[1-3] Recently, the practical applicability of photocatalytic systems in the near future compared to other competitive analogues (UV with H_2O_2 and/or O_3) in terms of efficiency, durability, and costs for material and system has been debated.[4] Heterogeneous oxide photocatalysts (e.g., TiO_2, ZnO, and WO_3) may exhibit a lower photo-efficiency than the UV-based homogeneous ones. However, the former works directly under natural sunlight whereas the latter essentially requires electricity (UV light) and auxiliary chemicals (H_2O_2, O_3, etc.). Although the photocatalyst materials are relatively cheap (e.g., ~$1 per kg for TiO_2) and durable,[4] they become more expensive and less durable when coupled with expensive, secondary materials (e.g., noble metals, graphenes, and polymers).[2-3] Post-recovery steps of used, suspended particles largely increase the operation cost of the photocatalytic system. More importantly, the periodic and abrupt fluctuations of sunlight further limit continuous operation of the system. All these factors make the photocatalysis less applicable as an independent process, inevitably requiring additional treatments.

With this in mind, we have long attempted to identify the functionality of particulate TiO_2 and WO_3 composite (TiO_2/WO_3, TW) films and apply them to energy production[5] and environmental cleanup.[6-8] In addition to their synthesis being simple and straightforward, TW films can work *without* i) any auxiliary, expensive materials, ii) post-separation process, and iii) even continuous sunlight. The last function is particularly unique in WO_3 that can store photogenerated electrons (photocharging process) and induce reduction in the following dark periods (discharging process).[7-11] Although TiO_2 itself also can act as an electron reservoir,[12-

[14] the interfacial electron transfer occurs quickly during the photocharging periods under oxic conditions and the application under the oxic conditions in the following dark periods is limited. On the other hand, inter-particle contact between WO_3 and other semiconductors with higher conduction bands (e.g., TiO_2 and CdS) significantly shortens the photocharging time due to additional electron supply via cascaded electron transfer while increasing the lifetime of stored electrons.[7-8] As-photocharged TW films have been successfully demonstrated to reductively convert metal ions (Cr^{6+} and Ag^{+}) and organic chemicals (e.g., methylene blue) with the stored electrons in the dark periods.[6-8,15]

We noted that the stored electrons can be transferred to dissolved O_2 followed by the production of reactive oxygen species (ROSs, e.g., $O_2^{\bullet-}$, $HO_2^{\bullet}$, and H_2O_2) which are capable of oxidizing substrates via a reductive pathway (**Scheme 1**). O_2 is the most ubiquitous electron acceptor in aqueous media. In addition, ROSs are environmentally clean oxidizing agents widely used in the treatment of (in)organic substrates.[3] This study attempted to apply the TW membrane filters to the oxidation of As(III) to As(V) by ROSs produced via a reductive pathway in the absence of any auxiliary chemicals under ambient conditions in the dark. To the best of our knowledge, this application has not been reported yet. Arsenic-contaminated drinking water has long caused serious problems such as skin lesions and skin cancer to human, particularly in developing countries with limited access to water treatment facilities.[16-17] Arsenite (As(III), H_3AsO_3; pK_a = 9.4, 12.1, and 13.4) is more toxic and difficult for removal than arsenate As(V) (H_3AsO_4) due to higher mobility and lower affinity for absorbents and coagulants in the former.[18-19] Although the photocatalytic As(III) oxidation mechanism should primarily follow an oxidative pathway with hydroxyl radicals ($^{\bullet}OH$) generated via the hole transfer, the reductive pathway mediated with ROSs has been proposed

to occur as well under irradiation.[20] In this study, the hole transfer (*i.e.*, $^{\bullet}$OH-mediation) was not directly involved in the discharging process and hence the reductive pathway with the stored electrons (*i.e.*, ROS mediation) should be predominant in the As(III) oxidation. This finding can further support the existence of a reductive pathway in the As(III) oxidation mechanism, which has long been debated.[20]

Experimental methods

Chemicals and materials. The following chemicals were used in this study: $NaAsO_2$ (As(III), Sigma-Aldrich), $Na_2HAsO_4{\cdot}7H_2O$ (As(V), Sigma-Aldrich), molybdate reagent solution (Sigma-Aldrich), methanol (MeOH, Merck), *p*-benzoquinone (BQ, Sigma-Aldrich), hydrochloric acid (Junsei), L-histidine (Sigma-Aldrich), superoxide dismutase (SOD, Sigma-Aldrich; from bovine erythrocytes), ascorbic acid (Sigma-Aldrich), ethanol (Merck), sodium hydroxide (Sigma-Aldrich), hydrogen peroxide (Duksan), SiO_2 (Sigma-Aldrich), WO_3 (Kanto, particle size of ~30 μm), and TiO_2 (Degussa P25 with a primary particle size of *approx.* 30 nm). All chemicals were of analytical grade and used as received. Ultrapure deionized water (18 MΩ cm) was used to prepare all aqueous solutions.

Preparation of photocharged membrane filters. To make composite TiO_2 and WO_3 (TW) particle-embedded membrane filters, TiO_2 and WO_3 particles were suspended in air-equilibrated aqueous solutions with ethanol (20 vol%) as a hole scavenger in TiO_2/WO_3 weight ratios of 1/0, 3/1, 1/1, 1/3, and 0/1 (denoted as TW100, TW75, TW50, TW25, and TW0, respectively) and stirred for 30 min. The suspension was filtered and washed and transferred to a mixed cellulose ester membrane filter (Merck, diameter: 47 mm, pore size: 0.45 μm, thickness: 150 μm) by vacuum filtration. The as-prepared thickness of TW filters

was estimated to be ~0.14 mm using a digital Vernier Caliper (Mitutoyo). The TW membrane was then irradiated (i.e., photocharged) with UV254 (SANYO, G6T5), UV365 (SANKYO, F6T5BLB), and air mass (AM) 1.5 light with an intensity of 100 mW cm^{-2} (1 sun; ABET) for varying times (0.5–5 h; typically, it was 1 h unless otherwise mentioned). The irradiation led to color change from green to dark blue and red-shift of the absorption edge (**Figure S1**), which is consistent with the results obtained in a previous study.[7]

Arsenic redox reaction and characterization. The photocharged TW membrane filters (typically, TW50 unless otherwise mentioned) were transferred to a filtration system for oxidizing As(III) to As(V) (**Figure S2**). Air-equilibrated aqueous As(III) solutions (typically, 0.1 mM in 90 mL at pH 5) passed through the charged TW filters at a flow rate 0.5 mL min^{-1} over 2 h using a peristaltic pump (Longer) in the absence of any irradiation. To examine the effect of dissolved O_2, N_2 gas was used to purge the feed solutions prior to and during the flow process. If necessary, pH of the feed solutions was initially adjusted using HCl and NaOH to examine the effect of pH on the As(IIII) oxidation kinetics. The filtered solutions were intermittently sampled and analyzed for As(V) concentrations (i.e., [As(V)]), which were then converted into the amounts of As(V) (= $[As(V)]_t \times$ flow rate $\times t$; where t is time). $[As(V)]_t$ in the filtered solution was colorimetically determined using molybdenum blue method.[21] In brief, 0.5 mL of the aliquot was added to a conical tube containing deionized water (2.2 mL), ascorbic acid (100 μL at 0.1 g mL^{-1}), and a molybdate reagent solution (200 μL, Sigma-Aldrich). The mixed solution was vigorously mixed and kept in an oven for 2 h at 40 °C; then, it was analyzed using a UV-visible spectrophotometer (Shimadzu, UV-2450) at λ = 870 nm (ε = 19,550 M^{-1} cm^{-1}).[21] In addition, an As(V) solution (instead of As(III)) passed through the charged TW and the amounts of As(III) produced via reduction of As(V)

were quantified using a high-performance liquid chromatography (HPLC, Waters 2695) instrument equipped with a Aminex HPX-87H ion exclusion column (Bio-Rad, 300 × 7.8 mm) and a dual absorbance detector (Waters 2487). A binary mixture of distilled water and sulfuric acid (5 mM) was used as a mobile phase at a flow rate of 0.6 mL min^{-1}. For comparison, the redox behavior of Cr(VI/III) pair with the charged TW membrane filters was examined (**Figure S3**).

The pore structures of the as-prepared TW samples were analyzed using a gas sorption analyzer (Autosorb-iQ & Quadrasorb SI, Quantachrome Instrument). The Brunauer-Emmett-Teller (BET) surface area of the TW composite particles was estimated to be 33.87 m^2 g^{-1}, and their average pore diameter and volume were 27.15 nm and 0.23 cc g^{-1}, respectively. The surface charge of the samples was also analyzed at pH 5 using an electrophoretic light scattering system (Zetasizer Nano ZS, Malvern). The zeta potentials of TiO_2, WO_3, and TiO_2/WO_3 particles were estimated to be +22.1, –29.4, and –20.1 mV, respectively. The diffuse reflectance (R) spectra of TW before and after photocharging was obtained using the spectrophotometer (Shimadzu, UV-2540) and converted into the absorbance using the Kubelka–Munk equation (Abs = $(1–R)^2/2R$). Time-resolved photoluminescence lifetime (TRPL) decays of non-charged and charged TW filters were obtained using a confocal microscope (MicroTime-200, Picoquant, Germany) with a 40× objective. The lifetime measurements were performed at the Korea Basic Science Institute (KBSI), Daegu Center, Korea. A single-mode pulsed diode laser (375 nm with 30 ps pulse width and 3–5 μW power) was used as an excitation source. Details of the analysis have been reported elsewhere.[22-23] Electron paramagnetic resonance (EPR) analysis was performed using 5,5-dimethyl-1-pyrroline *N*-oxide (DMPO, >97%, TCI) as the spin-trapping reagent for

153 $OH^{\bullet}$ and $O_2^{\bullet-}$ (or $HO_2^{\bullet}$). The EPR spectrometer (Bruker EMXplus-9.5/2.7) was operated with
154 a center field of 3,360 G, microwave frequency of 9.430 GHz, microwave power of 6.325
155 mW, modulation frequency of 100 kHz, and modulation amplitude of 5 G.

156 The maximum photon-to-charge storage efficiency (ϕ_{ps}), stored charge-to-As(III)
157 oxidation efficiency (ϕ_{sc}), and overall photoconversion efficiency (ϕ_{pc}, *i.e.*, in the dark) were
158 estimated as follows (Eqs. 1-4).

159 ϕ_{ps} = number of stored charges/number of incident photons × 100% (Eq. 1)

160 ϕ_{sc} = number of As(V) produced/number of stored charges × 100% (Eq. 2)

161 ϕ_{pc} = number of As(V) produced/number of incident photons × 100% (Eq. 3)

162 $\phi_{pc} = \phi_{ps} \times \phi_{sc}$ (Eq. 4)

163 The number of incident photons from UV254 was estimated using a well-known chemical
164 actinometer couple of iodide and iodate (assuming a quantum yield of 75%).[24] In addition,
165 the maximum storage capacity of WO_3 was assumed to be 115 mAh g^{-1} when a single charge
166 was stored as in the form of HWO_3.[25] TiO_2 was considered incapable of storing charges.
167

168 ## Results and discussion

169 ***Catalytic oxidation of As(III) using charged TW membrane filters.*** As-fabricated TW
170 membrane filters were pre-irradiated for 1 h using three different lamps (UV254, UV365, and
171 AM1.5) and transferred to a once-through flow-type system for redox reactions of As(V/III)
172 pair in the dark (**Figure S2**). As air-equilibrated As(V) solution passed through the TW filter
173 pre-charged with UV254, the maximum amount of As(III) ($[As^{III}]_{max}$) of ~0.2 μmol was
174 produced in 1 h in the filtered solution (**Figure 1a**).

N_2-purging of the As(V) solution enhanced the As(III) production by two times. The reduction of As(V) to As(III) is attributed to the well-known electron transfer from the charged TW to the As(V) (**R1**, where e^-_{TW} refers to stored electrons in the charged TW).

$$e^-_{TW} + 1/2As^{5+} \rightarrow 1/2As^{3+} \quad \text{(R1)}$$

Such charge transfer should be facilitated with N_2 purging due to the removal of the competing O_2 for the electron (i.e., $E°$[As(V/III) = ~+0.26 V at pH 5; $E°(O_2/HO_2^{\bullet})$ = –0.05 V].[26]

Notably, when air-equilibrated As(III) solutions (*instead of As(V)*) were passed through the charged TW, As(V) was continuously produced with a $[As^V]_{max}$ of ~0.15 μmol in 3 h in the absence of irradiation (**Figure 1b**). A similar time profile of As(V) production (but with a smaller $[As^V]_{max}$) was observed for the UV365-charged TW. Photocharging with AM1.5 light (100 mW cm^{-2}) led to the same $[As^V]_{max}$ as the that for UV254 despite slower kinetics. This indicates that the pre-charged TW membrane filters can be used *not only for As(V) reduction but also for As(III) oxidation in the dark*, regardless of the irradiation condition, as long as the TW is charged (*see* below for more discussion). As(V) was not produced with non-charged TW filters, indicating that the pre-charging is essential for As(III) oxidation. It is noteworthy that the As(V) production was markedly inhibited with N_2 purging, whereas it was enhanced with O_2 purging ($[As^V]_{max}$ ~0.2 μmol). This phenomenon is in contrast to the case of reduction of As(V) to As(III) (**Figure 1a**). Dissolved O_2 appears to mediate As(III) oxidation via various reactive oxygen species (ROSs) produced by the stored electrons. It should be noted that the contradictory role of O_2 in the As(V/III) redox reaction was not found in the case of Cr(VI/III). As shown in **Figure S3**, the reduction of Cr(VI) to

Cr(III) proceeded faster with N_2 purging than that with air, whereas the oxidation of Cr(III) to Cr(VI) hardly occurred both under N_2-purged and air-equilibrated conditions.

To speculate the ROSs responsible for the As(III) oxidation, air-equilibrated As(III) solutions with methanol (MeOH), *L*-histidine, superoxide dismutase (SOD), and *p*-benzoquinone (BQ) as scavengers of $OH^{\bullet}$ ($k = 3 \times 10^9$ M^{-1} s^{-1}),[27] $^1O_2$ ($k = 3 \times 10^7$ M^{-1} s^{-1}), $O_2^{\bullet-}$ ($k = 1 \times 10^9$ M^{-1} s^{-1}),[28] and $HO_2^{\bullet}$ ($k = 2 \times 10^9$ M^{-1} s^{-1}),[24] respectively, were passed through the charged TW filters (**Figure 2a**). The effects of MeOH and *L*-histidine on the As(V) production were insignificant, whereas the As(V) production was completely inhibited with SOD and BQ. Accordingly, the observed As(III) oxidation was presumed to proceed via the mediation of $HO_2^{\bullet}/O_2^{\bullet-}$ pairs (**R2-R5**).

$$e^-_{TW} + O_2 \rightarrow O_2^{\bullet-} \quad \text{(R2)}$$

$$2O_2^{\bullet-} + H_2O + As^{III}(OH)_3 \rightarrow OAs^{V}(OH)_3 + O_2 + 2OH^- \quad \text{(R3)}$$

$$e^-_{TW} + O_2 + H^+ \rightarrow HO_2^{\bullet} \quad \text{(R4)}$$

$$2HO_2^{\bullet} + As^{III}(OH)_3 \rightarrow OAs^{V}(OH)_3 + O_2 + H_2O \quad \text{(R5)}$$

Interestingly, a thermochemical comparison between the O_2 reduction potential ($E^0(O_2/O_2^{\bullet-})$ = –0.33 V; $E^0(O_2/HO_2^{\bullet})$ = –0.05 V)[29-30] and the CB edge of WO_3 (*approx*. +0.4 V, being more positive than TiO_2 at –0.1 V)[5,7] indicates that the above reactions are unlikely to occur (**Scheme 1**). However, the reduction potential of adsorbed O_2 can be different from that of free O_2. Even if the difference is not large enough and the CB edge of WO_3 (i.e., defect-free) is still unable to produce $HO_2^{\bullet}/O_2^{\bullet-}$ pairs from the adsorbed O_2, the (photo)chemical reduction of WO_3 (i.e., the formation of $Y_xW^{6-x}O_3$, where Y refers to cations such as Li^+, Na^+, and H^+) can shift the CB edge negatively (e.g., –0.15 V)[31-32] and produce ROSs.

219 The effect of pH was further examined since the CB edge shifts upward (*i.e.*, –59
220 mV per pH)[33] with increasing pH, making the charge transfer more feasible (**Scheme 1**). As
221 shown in **Figure 2b**, $[As^{V}]_{max}$ increased linearly with increasing pH (*approx*. 3-fold between
222 pH 2 and 8) (*see* **Figure S4** for time-profiles of the production). An increase in pH to over ~9
223 resulted in gradual dissolution of WO_3 and hence the pH was not increased beyond this point.
224 Notably, the protonated ROSs ($OH^{\bullet}$, $HO_2^{\bullet}$, and H_2O_2) undergo shifts in their redox potentials
225 as much as the ΔCB edge (*i.e.*, –59 mV per pH), nullifying the positive effect of pH. On the
226 other hand, the redox potential of $O_2^{\bullet-}$ is not influenced by pH due to the proton-free electron
227 transfer. This suggests that $O_2^{\bullet-}$ can be responsible for As(III) oxidation, even though
228 decoupling of $O_2^{\bullet-}$ and $HO_2^{\bullet}$ is technically difficult.
229 The EPR spin-trapping technique with DMPO was employed to confirm the
230 production of ROSs. As shown in **Figure 3a**, peaks associated with DMPO-OH and DMPO-
231 OOH (virtually indistinguishable from those for DMPO-$O_2^{\bullet-}$)[28,34] were found in the charged-
232 TW filters (indicated by * and o, respectively); the peak intensity grew with time due to
233 accumulation of the adducts. No specific peaks were observed for non-charged TW filters
234 (**Figure S5**), indicating the formation of the adducts attributable to the ROSs produced in the
235 charged TW filters. However, detection of the DMPO-OH adduct was rather unexpected
236 because methanol ($OH^{\bullet}$ scavenger) did not influence the As(III) oxidation kinetics (**Figure**
237 **2a**). Hence, SOD was added to the DMPO solution to re-confirm the production of $O_2^{\bullet-}$ (or
238 $HO_2^{\bullet}/O_2^{\bullet-}$ pair) in charged TW filters.[30] As expected, peaks of the DMPO-OOH adduct
239 vanished (**Figure 3b**); interestingly, peaks of the DMPO-OH adduct disappeared as well. The
240 same behavior of both adducts can be attributed to the transformation of $HO_2^{\bullet}/O_2^{\bullet-}$ pair into

241 $OH^{\bullet}$ via HOOH (**R6-R8**).[35] Removal of the former by SOD inhibits HOOH formation and
242 consequently $OH^{\bullet}$ formation.

243 $$O_2^{\bullet-} + 2H^+ + e^- \rightarrow H_2O_2 \quad \text{(R6)}$$

244 $$HO_2^{\bullet} + H^+ + e^- \rightarrow H_2O_2 \quad \text{(R7)}$$

245 $$H_2O_2 + H^+ + e^- \rightarrow OH^{\bullet} + H_2O \quad \text{(R8)}$$

246 However, H_2O_2 was not found in the filtered solutions regardless of the presence of
247 As(III), even though its formation was thermochemically possible ($E^0(O_2/H_2O_2)$ = +0.695
248 V).[26] It appears that the presence of As(III) inhibits the formation of HOOH (R6 and R7) due
249 to the preferential reaction with the $HO_2^{\bullet}/O_2^{\bullet-}$ pair (R3 and R5), whereas HOOH decomposed
250 into $OH^{\bullet}$ in the absence of As(III) (R8). $HO_2^{\bullet}/O_2^{\bullet-}$ pairs can be indirectly produced from the
251 decomposition of H_2O_2 via electron withdrawal from the O–O bond;[36] yet the pathway
252 appeared to play a minor role in the process. To examine the possible effect of H_2O_2, As(III)
253 solutions with various concentrations of H_2O_2 (0.01–0.1 mM) were passed through the *non-*
254 *charged* TW (**Figure S6**). As(V) production increased with increasing H_2O_2 concentration;
255 $[As^V]_{max}$ for a H_2O_2 concentration at 0.01–0.02 mM was similar as that for the charged TW
256 without added H_2O_2. This suggests that the pre-charging can have the same effect as H_2O_2
257 concentrations of 0.01 and 0.02 mM *only if* H_2O_2 is involved in the As(III) oxidation.

258

259 ***Storing charges in TiO_2/WO_3 composite membrane filters***.

260 We have examined the primary roles of TiO_2 and WO_3 in photocharging-discharging
261 processes. **Figure 4** shows the XPS spectra of W4f and Ti2p bands in TW membrane filters
262 before and after photocharing. Obviously, the photocharging shifted the W 4f bands (W $4f_{5/2}$

263 at ~36.7 eV and W $4f_{7/2}$ at ~34.7 eV) to a lower binding energy region by 0.5 eV. The W4f
264 bands in the used TW filter (*i.e.*, discharged one) shifted back to the original binding energy.
265 Such a reversible shift in the W4f band was found in the repeated As(III) oxidation cycles
266 (*see* **Figure 7**). On the other hand, the Ti 2p bands insignificantly shifted (Δ0.1 eV) in the
267 photocharging-discharging cycles. This indicates that the Ti^{4+} state was nearly unchanged,
268 whereas the $W^{6+/(6-x)+}$ redox reaction occurred reversibly in the photocharging-discharging
269 cycles. It appears that the photogenrated electrons are quickly transferred from TiO_2 to the
270 interfacial O_2 and/or WO_3, because the CB edge of TiO_2 is higher than the redox potential of
271 O_2 and the CB edge of WO_3. On the other hand, the CB edge of WO_3 is comparable to the O_2
272 redox potential and the unbalanced electron transfers between TiO_2/WO_3 (fast transfer) and
273 WO_3/O_2 (slow transfer) should result in the electron accumulation in WO_3 (*i.e.*, formation of
274 the $W^{(6-x)+}$ state) during the photocharging period. In the discharging period, the electron-
275 accumulated WO_3 transfers the electrons to interfacial O_2, shifting the $W^{(6-x)+}$ state to the W^{6+}
276 state.

277 With this knowledge in mind, we attempted to optimize the synthesis of TW
278 membrane filters and examine their applicability. **Figure 5a** shows the As(V) production
279 using TW filters (pre-charged with UV254 and AM 1.5 light for 1 h) as a function of the
280 weight ratio of TiO_2 and WO_3 (*see* **Figure S7** for time-profiles of the production). The
281 UV254-charged TiO_2 filters without WO_3 (i.e., TW 100) showed no activity toward As(III)
282 oxidation in the dark. As the WO_3 fraction increased, the As(V) production increased rather
283 linearly; however, with 100% WO_3 (TW 0), As(V) production decreased significantly. The
284 highest activity of TW25 (TiO_2/WO_3 = 1/3) was found in the case of AM 1.5 light (e.g., TW
285 25 vs. TW 50) as well. A large fraction of WO_3 can lead to broad absorption of AM 1.5 light

due to a narrower bandgap (E_g ~2.7 eV; λ < ~450 nm) than E_g of TiO_2 (E_g ~3.2 eV; λ < 400 nm, **Figure 5a inset**). However, the effect of TiO_2/WO_3 ratio cannot be simply explained in terms of the light absorption alone, because TW 25 was superior to TW 50 even when pre-charged with UV 254 (fully absorbed by both TiO_2 and WO_3). The significantly low activities of TW 0 (*i.e.*, 100% WO_3) and TW 100 (*i.e.*, 100% TiO_2) further suggest that both TiO_2 and WO_3 are essential as a supplier of photogenerated electrons and a reservoir, respectively. Hence, when the former role is limited, for example, by replacing TiO_2 with photo-inactive SiO_2 (*i.e.*, SiO_2/WO_3), then As(III) oxidation is significantly inhibited. In addition, if the role of the latter is removed, for example, using SiO_2 instead of WO_3 (i.e., TiO_2/SiO_2), then As(III) oxidation does not proceed (**Figure S8**).

An increase in photocharging time also can enhance As(V) production for a fixed TW ratio (i.e., TW 50). As shown in **Figure 5b**, As(V) production increased with increasing photocharging time (i.e., $[As^V_{max}]$ ~0.3 μmol in ~3 h; *see* **Figure S9** for time-profiles). As the photocharging continued, a light pale yellowish TW filter turned greenish blue in color (**Figure 5b inset**) due to reduction of W^{6+} to $W^{(6-x)+}$ in the WO_3. The reduced state of the TW filter was stable in the absence of suitable interfacial electron acceptors (e.g., O_2, Cr(VI), and methylene blue).[7] Time-resolved photoluminescence emission decay spectra (**Figure 5b inset**) further revealed that a photocharged TW filter showed a two-fold longer decay lifetime (τ) than that of a non-charged TW filter (τ ~14 and 33 ns for non-charged and charged TW filters, respectively). It appears that the photo-charging creates trap sites, where the photogenerated electrons are gradually transferred to interfacial O_2.

We attempted to quantitatively estimate the stored charge-to-As(III) oxidation efficiency ($\phi_{sc} = \phi_{pc} / \phi_{ps}$; see Eq. 4) of TW filters (pre-charged with UV 254 for 1 h). To do

this, TiO_2 was assumed to have no contribution to the charge storage. The maximum charge storage capacity of TW was dependent on the weight fraction of WO_3 (maximum 115 mAh g^{-1} when a single charge is stored in the form of HWO_3). The maximum photon-to-charge storage efficiency (ϕ_{ps}, as shown in Eq. 1) of WO_3 (i.e., TW 0) was ~4.5% and linearly decreased with increasing TW ratios (i.e., decreasing WO_3 fraction) (**Figure 6a**). In addition, the overall photoconversion efficiency (ϕ_{pc}; see Eq. 3) was estimated, even though all As(III) oxidation reactions were performed in the dark. ϕ_{pc} was found to be less than 1%, and TW 25 exhibited the highest value (**Figure 6b**). This value (estimated in the dark) must be distinguished from the conventional photoconversion efficiency estimated under continuous irradiation. For example, TW 25 can drive As(III) oxidation in the dark with ~0.65% of incident photons (irradiated for 1 h). The highest ϕ_{pc} value for TW 25 suggests that the storage ability of WO_3 is critical. Based on the as-obtained ϕ_{ps} and ϕ_{pc} values, ϕ_{sc} could be estimated (**Figure 6c**). Although WO_3 alone (TW 0) exhibited ϕ_{sc} of ~2.5%, significantly higher ϕ_{sc} values (15–20%) were observed for TiO_2 and WO_3 heterojunctions. The presence of TiO_2 should contribute to the charge transfer processes (i.e., generation, separation, and injection) and make WO_3 more reduced, which shifts the Fermi level of WO_3 and produces ROSs more effectively.

Finally, the maximum capacity of a 1 h-singly charged TW 50 filter for As(III) oxidation was examined. For this, a freshly prepared aqueous feed solution of As(III) was refilled after a previous cycle and passed through the same TW filter without additional charging. The As(V) production decreased gradually and completely disappeared in the fourth recycling (**Figure 7a**). The 1 h-singly charged TW 50 filter was estimated to oxidize a

total of ~0.25 μmol of As(III). On the other hand, recharging of TW in each cycle recovered and maintained the catalytic activities of As(III) oxidation and Cr(VI) reduction (**Figure 7b** and **S10**, respectively). Reversible change in the color and shift in the XPS W4f band of TW filters (**Figure 4**) confirm that TW filters are stable and recyclable. This indicates that i) the gradual deactivation can be attributed to the consumption of electrons stored in the TW during the multiple uses and ii) the TW filter system can be easily reused after a simple recharging process without the need of recovery of the catalysts during repeated use. The same crystalline structure (monoclinic for WO_3 and mixed anatase/rutile for TiO_2) between photocharged and discharged TW filters further confirms the durability (**Figure S11**). For comparison, TiO_2 and WO_3-mixed suspension systems were tested for As(III) oxidation under the same conditions as the TW filter system (**Figure S12**). The initial activity of the suspension was higher than that of the filter due to agitation-enhanced O_2 diffusion. However, a larger As(V) was produced in the filter system in the latter stage because a firm interparticle contact of TiO_2 and WO_3 was created in the filter whereas the suspension system underwent segregation of TiO_2 and WO_3.

In summary, pre-charged TiO_2 and WO_3 (TW)-embedded inorganic membrane filters are demonstrated to be capable of oxidizing As(III) to As(V) under ambient dark conditions without any auxiliary chemical additives. The electrons accumulated in the TW composite filters during the charging period are transferred to interfacial O_2, effectively forming ROSs, represented by $HO_2^{\bullet}$ and $O_2^{\bullet-}$. The involvement of these species was confirmed with the corresponding quenchers and spin-trapping reagents; although not identified, H_2O_2 appeared to indirectly contribute to As(III) oxidation. The pre-charging time and TW ratios significantly influence the As(III) oxidation; the latter is particularly critical because WO_3

354 contributes to not only charge generation but also charge storage. The charged TW membrane
355 system can be reused after recharging without disassembling the catalyst membrane. The
356 proposed As(III) oxidation process using the proposed system is applicable to and
357 environmentally benign in the continuous treatment of As(III)-contaminated water during
358 periods of unavailability of sunlight (e.g., cloudy and night-time conditions).
359

360 ## Acknowledgements

361 This research was partly supported by the National Research Foundation of Korea
362 (2019R1A2C2002602, 2018R1A6A1A03024962, and 2019M1A2A2065616). We are
363 grateful to the Global Research Laboratory (GRL) Program (2014K1A1A2041044)
364 through the National Research Foundation, Korea. This publication was made possible by
365 a grant from the Qatar National Research Fund under its National Priorities Research
366 Program (NPRP 10-1210-160019).
367

368 ## Supporting Information Available.

369 Digital photo and absorption spectra of TW before and after photocharging (Fig. S1), Photo
370 and scheme of a once-through filtration system (Fig. S2), Time-changes of the amounts of
371 Cr(III) and Cr(VI) (Fig. S3), Effect of initial solution pH on As(III) oxidation (Fig. S4),
372 Time-changes in the EPR spectra with non-charged TW filters (Fig. S5), Effect of H_2O_2 on
373 As(III) oxidation (Fig. S6), Time profiles of As(III) oxidation by charged TW membrane with
374 different TW rations (Fig. S7), Time profiles of As(III) oxidation on TiO_2/WO_3, TiO_2/SiO_2,
375 and WO_3/SiO_2 filters (Fig. S8), Effect of photocharging time of TW on As(III) oxidation (Fig.

S9), Repeated runs of Cr(VI) reduction using TW filter photocharged every 3 h (Fig. S10), XRD patterns of TW filters as-synthesized, photocharged, discharged, and re-photocharged (Fig. S11), Time profiles of As(III) oxidation using membrane filter and suspension system of TW 25 (Fig. S12). This information is available free of charge via the Internet at http://pubs.acs.org/.

References

1. Hoffmann, M. R.; Martin, S. T.; Choi, W.; Bahnemann, D. W., Environmental applications of semiconductor photocatalysis. *Chem. Rev.* **1995,** *95*, 69-96.
2. Park, H.; Kim, H.-i.; Moon, G.-h.; Choi, W., Photoinduced charge transfer processes in solar photocatalysis based on modified TiO_2. *Energy Environ. Sci.* **2016,** *9*, 411-433.
3. Park, H.; Park, Y.; Kim, W.; Choi, W., Surface modification of TiO_2 photocatalyst for environmental applications. *J. Photochem. Photobiol.C* **2013,** *15*, 1-20.
4. Loeb, S. K.; Alvarez, P. J. J.; Brame, J. A.; Cates, E. L.; Choi, W.; Crittenden, J.; Dionysiou, D. D.; Li, Q.; Li-Puma, G.; Quan, X.; Sedlak, D. L.; Waite, T. D.; Westerhoff, P.; Kim, J. H., The technology horizon for photocatalytic water treatment: Sunrise or sunset? *Environ. Sci. Technol.* **2019,** *53*, 2937-2947.
5. Park, H.; Bak, A.; Jeon, T. H.; Kim, S.; Choi, W., Photochargeable and dischargeable TiO_2 and WO_3 heterojunction electrodes. *Appl. Catal. B* **2012,** *115-116*, 74-80.
6. Han, D. S.; Elshorafa, R.; Yoon, S. H.; Kim, S.; Park, H.; Abdel-Wahab, A., Sunlight-charged heterojunction TiO_2 and WO_3 particle-embedded inorganic membranes for night-time environmental applications. *Photochem. Photobiol. Sci.* **2018,** *17*, 491-498.
7. Kim, S.; Park, H., Sunlight-harnessing and storing heterojunction $TiO_2/Al_2O_3/WO_3$ electrodes for night-time applications. *RSC Adv.* **2013,** *3*, 17551-17558.
8. Kim, S.; Park, Y.; Kim, W.; Park, H., Harnessing and storing visible light using a heterojunction of WO_3 and CdS for sunlight-free catalysis. *Photochem. Photobiol. Sci.* **2016,** *15*, 1006-1011.
9. Ngaotrakanwiwat, P.; Tatsuma, T.; Saitoh, S.; Ohko, Y.; Fujishima, A., Charge–discharge behavior of TiO_2–WO_3 photocatalysis systems with energy storage ability. *Phys. Chem. Chem. Phys.* **2003,** *5*, 3234-3237.
10. Tatsuma, T.; Saitoh, S.; Ngaotrakanwiwat, P.; Ohko, Y.; Fujishima, A., Energy storage of TiO_2−WO_3 photocatalysis systems in the gas phase. *Langmuir* **2002,** *18*, 7777-7779.
11. Tatsuma, T.; Saitoh, S.; Ohko, Y.; Fujishima, A., TiO_2-WO_3 photoelectrochemical anticorrosion system with an energy storage ability. *Chem. Mater.* **2001,** *13*, 2838-2842.

12. Mohamed, H. H.; Dillert, R.; Bahnemann, D. W., Reaction dynamics of the transfer of stored electrons on TiO_2 nanoparticles: A stopped flow study. *J. Photochem. Photobiol., A* **2011,** *217*, 271-271.
13. Mohamed, H. H.; Mendive, C. B.; Dillert, R.; Bahnemann, D. W., Kinetic and mechanistic investigations of multielectron trasnfer reactions induced by stored electrons in TiO_2 nanoparticles: A stopped flow study. *J. Phys. Chem. A* **2011,** *115*, 2139-2147.
14. Mohamed, H. H.; Dillert, R.; Bahnemann, D. W., TiO_2 nanoparticles as electron pools: Single- and multi-step electron transfer processes. *J. Photochem. Photobiol., A* **2012,** *245*, 9-17.
15. Zhao, D.; Chen, C.; Yu, C.; Ma, W.; Zhao, J., Photoinduced electron storage in WO_3/TiO_2 nanohybrid material in the presence of oxygen and postirradiated reduction of heavy metal ions. *J. Phys. Chem. C* **2009,** *113*, 13160-13165.
16. Karagas, M. R.; Gossai, A.; Pierce, B.; Ahsan, H., Drinking water arsenic contamination, skin lesions, and malignancies: A systematic review of the global evidence. *Cur. Environ. Health Rep.* **2015,** *2*, 52-68.
17. Korte, N. E.; Fernando, Q., A review of arsenic(III) in groundwater. *Crit. Rev. Environ. Control* **1991,** *21*, 1-39.
18. Kim, D.-h.; Bokare, A. D.; Koo, M. s.; Choi, W., Heterogeneous catalytic oxidation of As(III) on nonferrous metal oxides in the presence of H_2O_2. *Environ. Sci. Technol.* **2015,** *49*, 3506-3513.
19. Moon, G.-h.; Kim, D.-h.; Kim, H.-i.; Bokare, A. D.; Choi, W., Platinum-like behavior of reduced graphene oxide as a cocatalyst on TiO_2 for the efficient photocatalytic oxidation of arsenite. *Environ. Sci. Technol. Lett.* **2014,** *1*, 185-190.
20. Choi, W.; Yeo, J.; Ryu, J.; Tachikawa, T.; Majima, T., Photocatalytic oxidation mechanism of As(III) on TiO_2: Unique role of As(III) as a charge recombinant species. *Environ. Sci. Technol.* **2010,** *44*, 9099-9104.
21. Lenoble, V.; Deluchat, V.; Serpaud, B.; Bollinger, J.-C., Arsenite oxidation and arsenate determination by the molybdene blue method. *Talanta* **2003,** *61*, 267-276.
22. Jeong, H. W.; Chae, W.-S.; Song, B.; Cho, C.-H.; Baek, S.-H.; Park, Y.; Park, H., Optical resonance and charge transfer behavior on patterned WO_3 microdisc arrays. *Energy Environ. Sci.* **2016,** *9*, 3143-3150.
23. Kang, U.; Park, H., A facile synthesis of $CuFeO_2$ and CuO composite photocatalyst films for production of liquid formate from CO_2 and water over a month. *J. Mater. Chem. A* **2017,** *5*, 2123-2131.
24. Rahn, R. O.; Stefan, M. I.; Bolton, J. R.; Goren, E.; Shaw, P.-S.; Lykke, K. R., Quantum yield of the iodide-iodate chemical actinometer: Dependence on wavelength and concentration. *Photochem. Photobiol.* **2003,** *78*, 146-152.
25. Chen, Z.; Peng, Y.; Liu, F.; Le, Z.; Zhu, J.; Shen, G.; Zhang, D.; Wen, M.; Xiao, S.; Liu, C.-P.; Lu, Y.; Li, X., Hierarchial nanostructured WO_3 with biomimetic proton channels and mixed ionic-electronic conductivity for electrochemical energy storage. *Nano Lett.* **2015,** *15*, 6802-6808.
26. Lide, D. R., *CRC Handbook of Chemistry and Physics*. 90th ed.; CRC Press: New York, 2009.

27. Buxton, G. V.; Greenstock, C. L.; Helman, W. P.; Ross, A. B., Critical review of rate constants for reactions of hydrated electrons, hydrogen atoms and hydroxyl radicals in aqueous solution. *J. Phys. Chem. Ref. Data* **1988,** *17*, 513-886.
28. Bielski, B. H. J.; Cabelli, D. E.; Arudi, R. L.; Ross, A. B., Reactivity of HO_2/O_2^- radicals in aqueous solution. *J. Phys. Chem. Ref. Data* **1985,** *14*, 1041-1100.
29. Sawyer, D. T.; Valentine, J. S., How super is superoxide? *Acc. Chem. Res.* **1981,** *14*, 393-400.
30. Hayyan, M.; Hashim, M. A.; AlNashef, I. M., Superoxide ion: Generation and chemical implications. *Chem. Rev.* **2016,** *116*, 3029-3085.
31. Paik, T.; Cargnello, M.; Gordon, T. R.; Zhang, S.; Yun, H.; Lee, J. D.; Woo, H. Y.; Oh, S. J.; Kagan, C. R.; Fornasiero, P.; Murray, C. B., Photocatalytic hydrogen evolution from substoichiometric colloidal WO_{3-x} nanowires. *ACS Energy Lett.* **2018,** *3*, 1904-1910.
32. Yousaf, A. B.; Imran, M.; Zaidi, S. J.; Kasak, P., Highly efficient photocatalytic Z-scheme hydrogen production over oxygen-deficient WO_{3-x} nanorods supported $Zn_{0.3}Cd_{0.7}S$ heterostructure. *Sci. Rep.* **2017,** *7*, 6574.
33. Finklea, H. O., *Semiconductor Electrodes*. Elsevier: Amsterdam, 1988.
34. Buettner, G. R., On the reaction of superoxide with DMPO/OOH. *Free Rad. Res. Comms.* **1990,** *10*, 11-15.
35. Park, Y.; Kim, C.; Kim, M.; Kim, S.; Choi, W., Ambient-temperature catalytic degradation of aromatic compounds on iron oxide nanords supported on carbon nanofiber sheet. *Appl. Catal. B* **2019,** *259*, 118066.
36. Arends, I. W. C. E.; Sheldon, R. A., Recent developments in selective catalytic epoxidations with H_2O_2. *Top. Catal.* **2002,** *19*, 133-141.

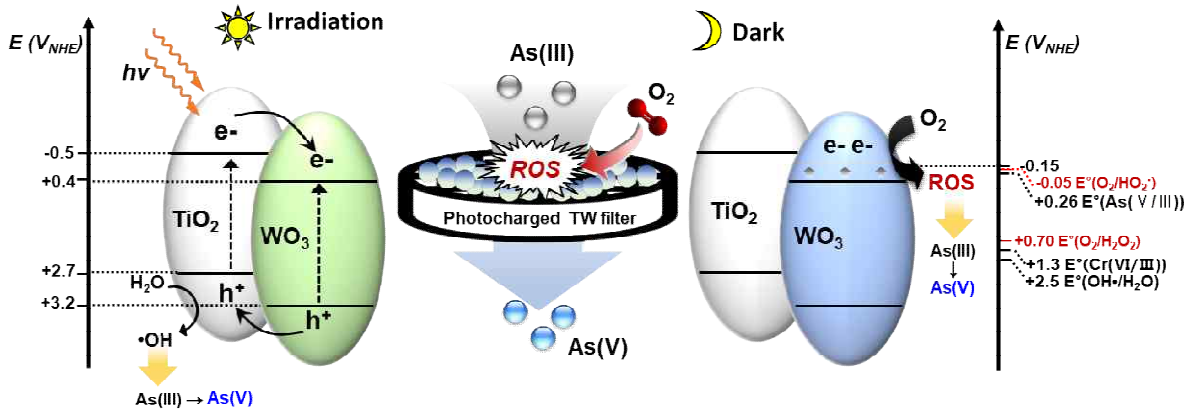

478

479 **Scheme 1**. Illustration of As(III) oxidation reactions occurring in TiO_2/WO_3 (TW) memb
480 rane filters under irradiation (left) and in the subsequent dark periods (right). ROS refers
481 to reactive oxygen species.

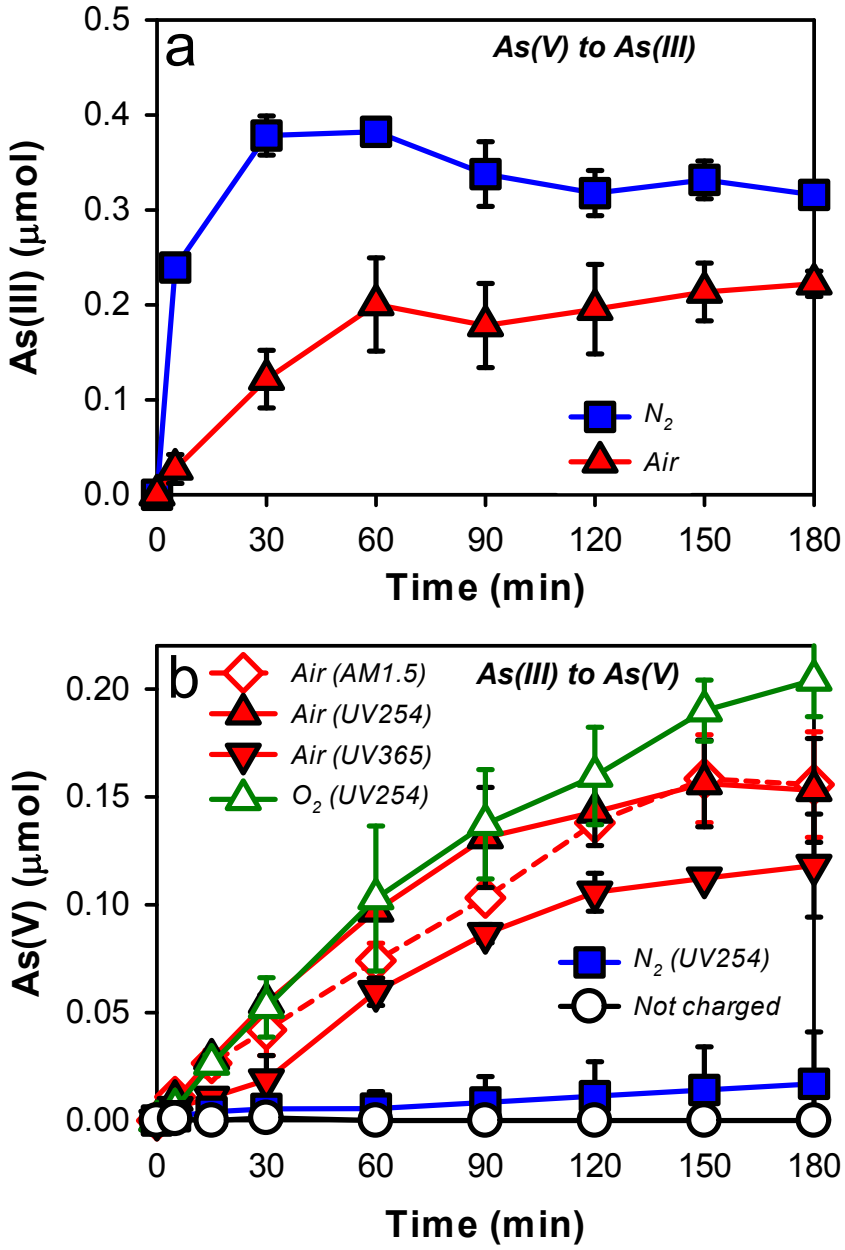

482

483 **Figure 1**. Time profiles of (a) As(III) production in aqueous solutions of As(V) (pH 5) and (b)
484 As(V) production in aqueous solutions of As(III) (pH 5) under ambient conditions in the dark.
485 In (a), air-equilibrated and N_2-purged solutions with 0.1 mM As(V) solutions flowed at a rate
486 of 0.5 mL min^{-1} through TW filters that were pre-charged for 1 h with UV 254 nm. In (b), 0.1
487 mM As(III) solutions that were equilibrated with air and purged with O_2 and N_2 were passed
488 through pre-charged TW filters (for 1 h with UV 254 nm, UV 365 nm, and AM 1.5 light).
489 While the solutions flowed, light was turned off. For comparison, the air-equilibrated As(III)
490 solution flowed through non-charged TW.

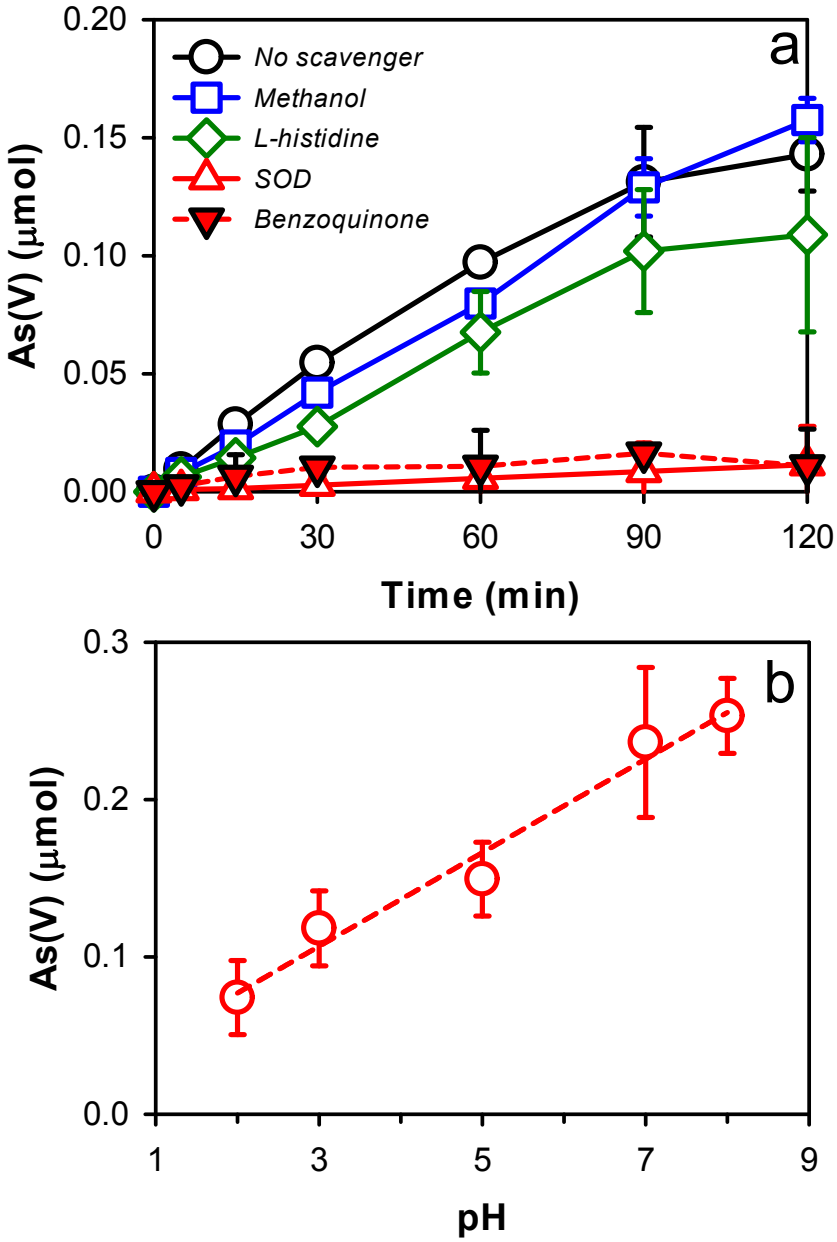

491

492 **Figure 2**. Effect of (a) ROS scavengers and (b) pH on the oxidation of As(III) to As(V). In
493 (a), air-equilibrated As(III) solutions with methanol (100 mM), L-histidine (100 mM), SOD
494 (55.11 mg L^{-1}), and *p*-benzoquinone (100 mM) as scavengers of $^{\bullet}OH$, $^{1}O_2$, $O_2^{\bullet-}$, and $HO_2^{\bullet}$,
495 respectively, flowed through pre-charged TW filters (for 1 h with UV 254). In (b), air-
496 equilibrated As(III) solutions (0.1 mM) with various pH flowed through pre-charged TW
497 filters.

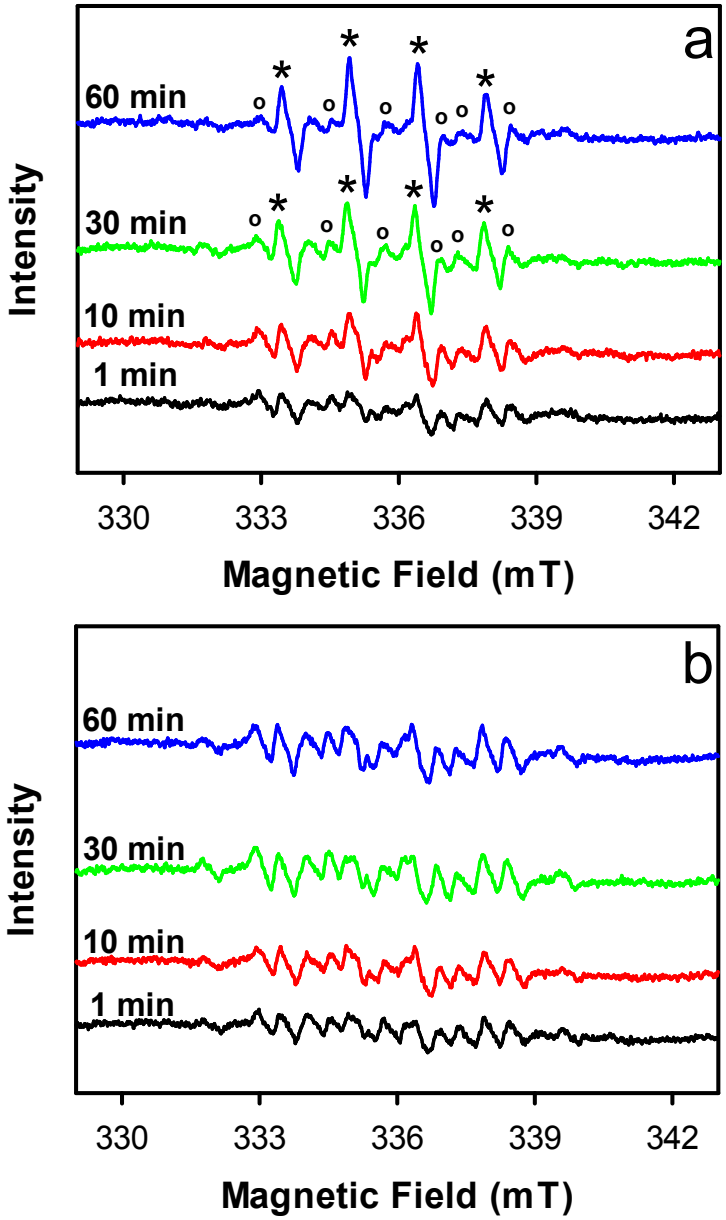

498

499 **Figure 3.** Time profiles of EPR spectra of DMPO solutions (a) without and (b) with SOD
500 flowed through charged TW filters. Symbols "∗" and "o" represent the peaks of DMPO-OH
501 and DMPO-OOH and adducts, respectively. $[DMPO]_0$ = 0.15 M; $[SOD]_0$ = 66.7 mg L^{-1}; TW
502 pre-charged for 2 h with UV254.

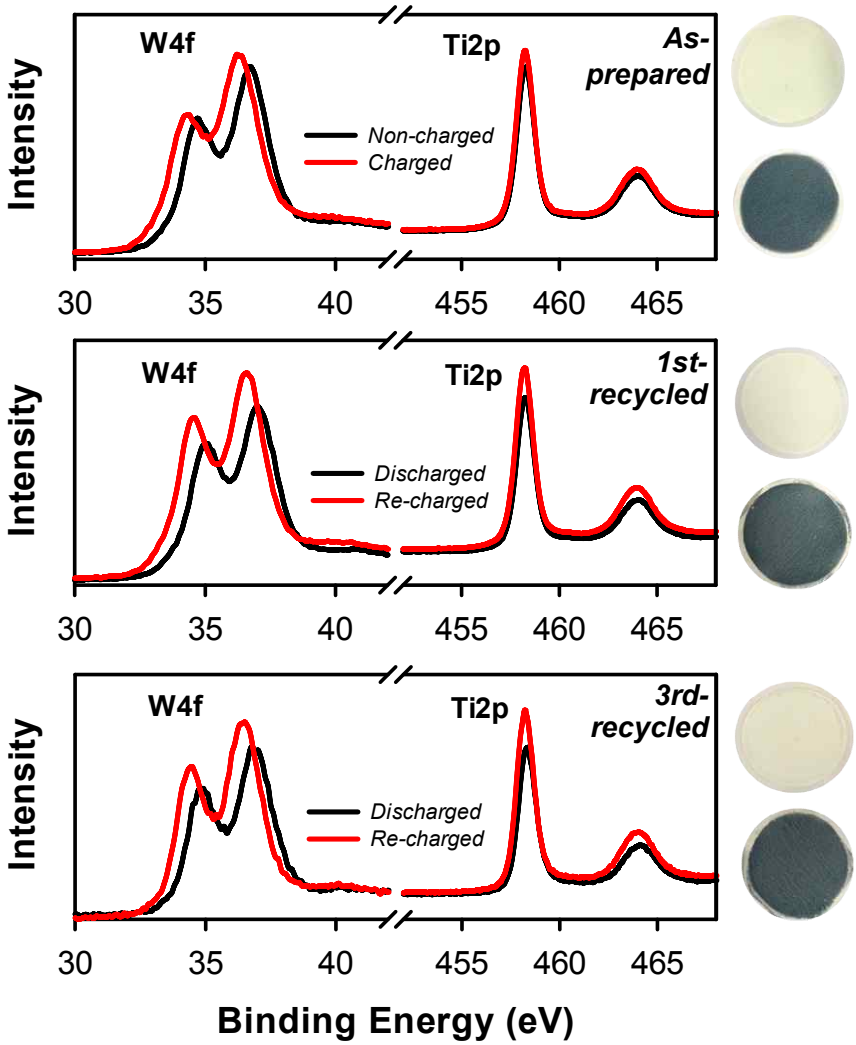

503

504 **Figure 4**. XPS spectra of W4f and Ti2p bands in as-prepared and recycled TW filters. The
505 as-photocharged TW sample was used (i.e., discharged) for As(III) oxidation (*see* **Figure 7**);
506 then the discharged TW sample was re-charged and reused (i.e., discharged) for As(III)
507 oxidation. This recycle was repeated three times. The photos show the non-charged and
508 charged TW filters (as-prepared), and discharged and recharged TW filters (1st and 3rd-
509 recycled).

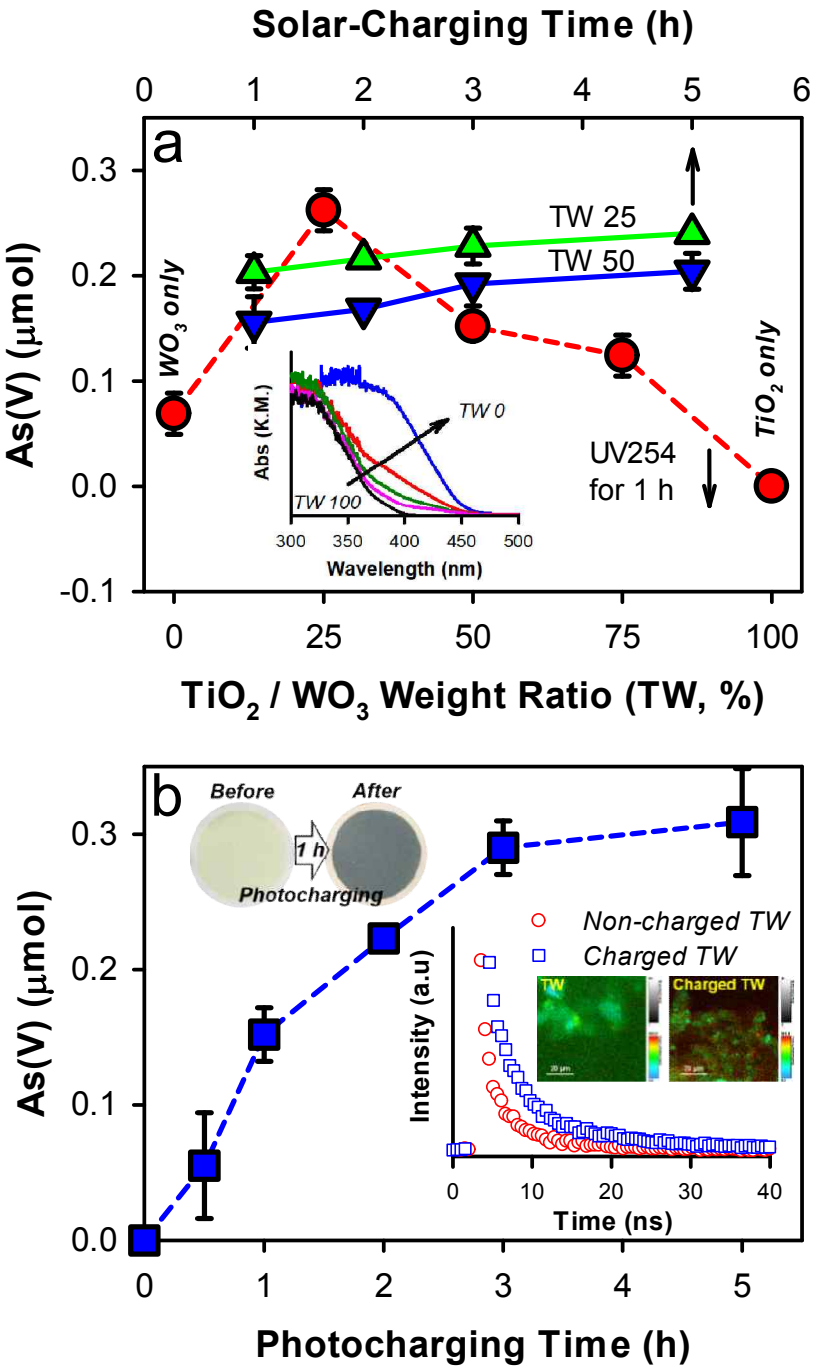

510

511 **Figure 5**. Effect of (a) TW weight ratio and (b) photocharging time on As(V) production (pH
512 5). The inset in Figure 4b shows time-resolved photoluminescence emission spectra of TiO_2
513 (T), WO_3 (W), and TiO_2/WO_3 (TW, non-charged and charged) films. Excited at λ = 375 nm.

514

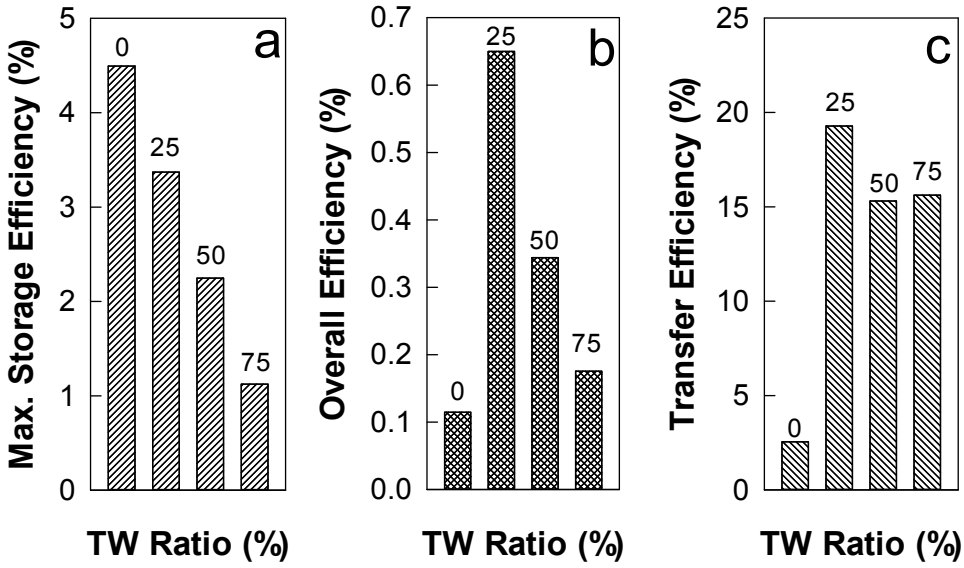

515 **Figure 6**. Effect of TiO_2 and WO_3 (TW) ratio on (a) the maximum charge storage efficiency,
516 (b) the overall incident photon-to-As(III) oxidation efficiency in the dark, and (c) the stored
517 charge-to-As(III) oxidation efficiency. TW filters were pre-charged with UV 254 nm for 1 h
518 (*approx*. 5.23×10^{19} photons, 4% deviation).

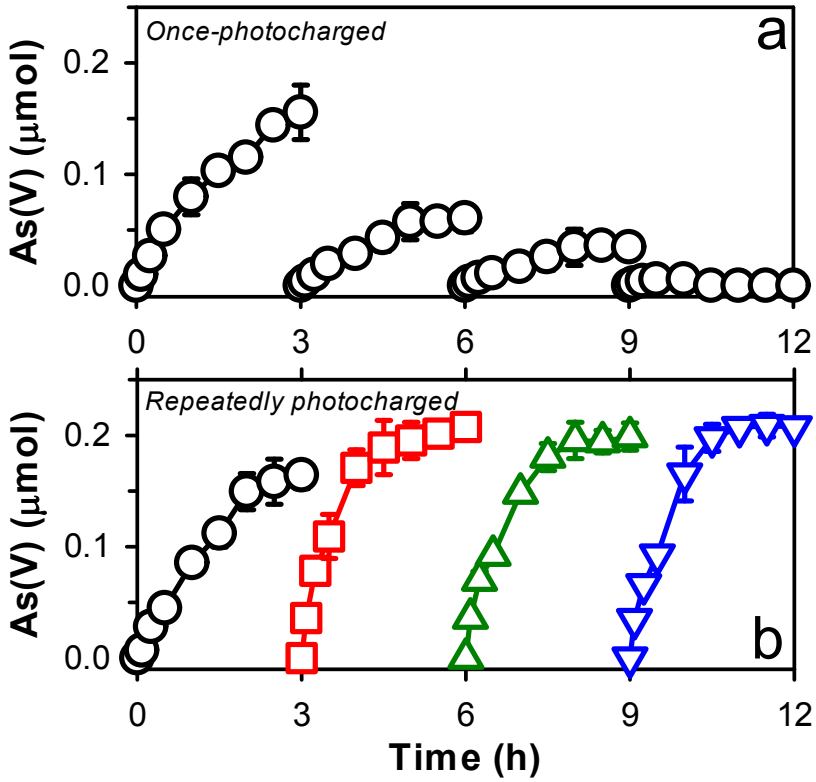

519

520 **Figure 7.** Repeated runs of As(III) oxidation using (a) singly photocharged TW filter and (b)
521 TW filter photocharged every 3 h (pH_i = 5.0, $[As(III)]_i$ = 0.1 mM, air-equilibrated). The
522 photocharging time was 1 h with UV 254.

Table of Contents